

Pedestrian Attribute Recognition in Video Surveillance

Scenarios Based on View-attribute Attention Localization

Weichen Chen¹ Xinyi Yu¹ Linlin Ou¹

¹ Collage of Information Engineering, Zhejiang University of Technology, Hangzhou 310023, China

Abstract: Pedestrian attribute recognition in surveillance scenarios is still a challenging task due to inaccurate localization of specific attributes. In this paper, we propose a novel view-attribute localization method based on attention (VALA), which relies on the strong relevance between attributes and views to capture specific view-attributes and to localize attribute-corresponding areas by attention mechanism. A specific view-attribute is composed by the extracted attribute feature and four view scores which are predicted by view predictor as the confidences for attribute from different views. View-attribute is then delivered back to shallow network layers for supervising deep feature extraction. To explore the location of a view-attribute, regional attention is introduced to aggregate spatial information of the input attribute feature in height and width direction for constraining the image into a narrow range. Moreover, the inter-channel dependency of view-feature is embedded in the above two spatial directions. An attention attribute-specific region is gained after fining the narrow range by balancing the ratio of channel dependencies between height and width branches. The final view-attribute recognition outcome is obtained by combining the output of regional attention with the view scores from view predictor. Experiments on three wide datasets (RAP, RAPv2, PETA, and PA-100K) demonstrate the effectiveness of our approach compared with state-of-the-art methods.

Keywords: Pedestrian attribute recognition, surveillance scenarios, view-attribute, attention mechanism, localization.

1 Introduction

With the expansion of surveillance technology, video surveillance system has been widely used in many domain, e.g., security, criminal investigation and traffic. Pedestrian attribute recognition in video surveillance has its great potential, which also facilitates the evolvement of person retrieval and person re-identification. Pedestrian attribute recognition is aiming to make predictions for a group of attributes, e.g., gender, age, wearing dress. Recently, methods^[2,3] based on convolutional neural networks (CNN) achieve great success in recognizing pedestrian attributes.

However, there still exist some difficulties and challenges in pedestrian attribute recognition, such as multi-view change, low resolution, low illumination, and occlusion in complex backgrounds. A solution is to guide the recognizing process via prior knowledge. Previous works^[3-5] attempt to take body part or pose information as prior knowledge to supervise learning. Bourdev et al.^[4] consider a recognition network based on body-part detector to construct attributes classification units. Similarly, Li et al.^[3] employ human posture as prior knowledge to locate body-related region for attribute recognition. However, these methods highly depend on the location of body parts. Incorrect positioning of body parts provides wrong features for attribute recognition, which may bring extra inferring time and computational cost.

Since images are recorded by monitoring cameras, multi-view change is the most severe challenge. Several associated problems can be caused by viewpoints change as each attribute of the identical pedestrian may be lain in different regions based on different views of images. As depicted in

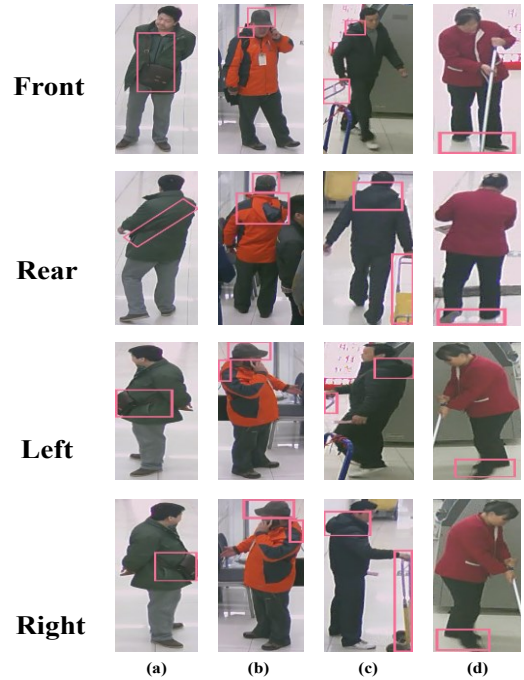


Fig. 1 Images of the same pedestrian identity from different views. (a-d) Example images of pedestrian attribute recognition are from RAPv2 dataset^[1], and typical attributes including single shoulder bag, shoes and hat are marked by pink bounding boxes.

Fig. 1, the spatial areas of hat attribute (group(b)) are larger in side views (3rd row and 4th row) than in the front view (1st row). On the contrary, the front view is more important for single shoulder bag attribute in group(a). When the relationship between each pedestrian attribute and different

views is known, it can be utilized as prior knowledge to guide the training process to focus on regions for each specific attribute. Therefore, in addition to the application of taking body parts as prior knowledge, view information can be considered as another efficient clue to compose specific view attribute for attribute recognition.

To get the location of view attribute more precisely, attention mechanism^[6-8] is introduced in recent methods. These methods^[7,8] usually yield attention masks from certain layers and then multiply them to corresponding feature maps for giving the position of attributes. As shown in Fig. 2(b), the learned attention mask attends a broad region and points out shirt, backpack and jeans attributes. However, the attention mask is inaccurate for a specific attribute and mix the regions of different attributes together for the reason of dealing with spatial information and channel inter-dependencies insufficiently. Later studies^[9,10] demonstrate the decisive capabilities of channel attention and positional information to generate attentive regions. Concretely speaking, SE-Net^[9] receives the cross-channel relationships in feature maps by learning per-channel modulation weights. This was followed by CBAM^[10] which enriches the attentive regions by adding max pooled features for the channel attention along with an added spatial attention component in two processes. As illustrated in Fig. 2(c,d), when recognizing Jeans, attentive regions produced by SE-Net^[9] and CBAM^[10] focus on specific position of Jeans. Nevertheless, SE-Net^[9] only considers the important of channel, and both of them^[9,10] reduce the channel dimension. Hence, these two modules are more likely to cause information loss, and the generated attention areas have deviations to some extent. To avoid feature loss and preserve spatial attribute information, two processes from CBAM^[10] are fused into one in our attention branch.

A novel method is proposed in this paper, namely View-attribute Localization based on Attention (VALA), which exports view prediction and attribute inference of pedestrian images recorded by surveillance cameras. By making full use of the differences among related areas of the identical attribute from different views, view information is adopted as prior knowledge to guide the training process to focus on specific attributes. Additionally, view information is holistic, so a view predictor is placed in shallow layers to gain holistic view confidences (incl. front, rear, left, right) for low-level features. Subsequently, view-confidences are combined with shallow features to form specific view-attribute. As view-attributes are existed, regional attention is proposed to restrict pedestrian position into a frame first, and then to localize view-attribute regions. Specifically, regional attention is divided into three small branches: height branch, width branch and ratio-balance branch. The first two branches are responsible for embedding spatial attribute information of feature maps along height dimension and width dimension to get a coarse domain, and channel inter-dependencies are captured after aggregating spatial information from two spatial dimensions. Then two attention maps are generated as the regional weights which can be combined with the output of the ratio-balance branch via multiplication

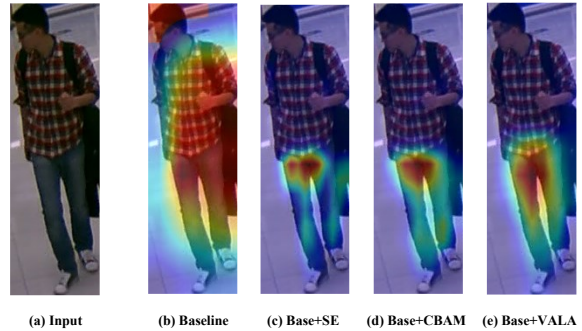


Fig. 2 Visualization of attribute attentive areas produced by different attention modules. (a) The example image of pedestrian attribute recognition is from RAPv2 dataset^[1]. (b-d) Visualization of the jeans attribute attention-related regions generated by a single baseline (refer to ResNet50^[11] here), SE module^[9], CBAM module^[10] and our VALA module respectively.

to receive a fine attribute-related region. Finally, the evaluating result is obtained by multiplying the confidences of global view-attribute with the attentive recognition outcome.

The contributions of this paper are presented as follows:

- We establish an end-to-end trainable framework which takes view information as prior knowledge to compose specific view-attribute in deep network supervision.
- We propose a regional attention to further localize specific view-attribute rather than classify attribute-regions from different views by manual operation.
- We conduct extensive experiments on three publicly pedestrian attribute recognition datasets, i.e. RAP^[12], RAPv2^[1], and PA-100K^[13], which clearly illustrate the competitive generalization ability and potentiality of our method.

2 Related Work

2.1 Pedestrian Attribute Recognition

Early pedestrian attribute recognition methods such as HOG^[14], SVM^[15] focus on hand-crafted features, but the performance of these traditional methods is far from satisfactory. With the rapid development of convolution neural network, recent methods based on CNNs achieve great success.

These methods^[2,3,5,6,8,16,17,18,19,20] can be classified into five categories:

Global-based: ACN^[2] used a CNN model to jointly learn and calculate loss for each attribute. DeepMAR^[16] regarded attribute learning as a multi-label task, and computed the loss of all attributes via sigmoid cross-entropy loss. However, global-based methods are out of application due to the lack of consideration of local fine-grained features.

Part-based: PGDM^[3] adopted a pose estimation model to localize human body parts. LG-Net^[5] applied EdgeBoxes^[21] to generate region-proposals for local features. DTM+AWK^[17] leveraged pose keypoints as auxiliary information to help the main module for proper attribute-

region. These methods that taking body-part and posture information as prior knowledge improve the performance a lot, but bring extra inferring time and computational cost from part localization modules.

Sequential-based: JRL^[18] exploited the inter-dependency among attributes to joint recurrent learning by a CNN-RNN model. GRL^[19] explored the intra-group and inter-group relationships of attributes, and divided all attributes into several groups to recognize. However, modules of these methods are usually more complicated and parameters are hard to control.

Attention-based: DIAA^[6] introduced a multi-scale visual attention to deal with the problem of attribute imbalance. DaHAR^[8] carried a coarse-to-fine attention mechanism to reduce irrelevant distraction areas and to improve the discriminative power for attribute recognition. As mentioned in Section 1, attention-based methods are always influenced by complex backgrounds and surroundings, which make attention masks fail to obtain the position of a specific attribute.

Attribute-based: ALM^[20] induced a localizing method for specific attribute to discover the most discriminative attribute regions.

Later studies are dedicated to solving the problems in pedestrian attribute recognition, but there is still likely to have many aspects for improving the recognizing performance in the future. Presently, attention of investigators gradually diverts from localizing generic attribute to specific attribute. Our method aims at proposing regional attention to localize composed specific view-attribute for the purpose of achieving great attribute recognition effect.

2.2 Multi-view Information

Besides occlusion and blurring, viewpoint change problem is difficult to handle. Since the related regions of a same attribute are in different positions from different views, it seems to have a relationship between attributes and views. Therefore, by making full use of the relationship, visual clues can be captured as auxiliary supervision to help attribute localization. Some methods^[22-24] attempt to leverage viewpoint information in different fields. As views are holistic, the parameters of networks are shared across all views which cause partial view-specific information to be ignored during feature extraction stages. Feng et al.^[22] offered a view-specific deep network which extracts the view clues more comprehensively to verify greater performance of view-feature model than generic-feature model in re-identification field. Multi-view information is also considered in face verification domain. Farfadi et al.^[23] proposed a deep dense face detector to detect faces in a wide range of views and discovered that different views can help detection handle occlusion and capture more features to some extent. In sentiment analysis research, Sadr et al.^[24] decided to combine features extracted from heterogeneous neural networks by using multi-view classifiers to enhance overall performance of document-level sentiment analysis. Our method takes view information as prior knowledge in

pedestrian attribute recognition field. View information in our paper is predicted from view branch to make up view-features, which can guide deep feature extraction process to focus on specific attributes.

2.3 Attention Localization

When observing a specific attribute in daily life, people are always involved in most relevant resource of input images, but ignore the interference of irrelevant areas. Originated from human visual behaviors, attention mechanism is introduced to pay more attention to attribute-related region. Zhu et al.^[25] firstly applied the attention mechanism to pedestrian attribute recognition and revealed that increasing the weights of attentive attribute regions can focus on the most representative attribute features^[26]. Liu et al.^[13] carried an attentive module to fuse multi-scale features from multiple levels to yield attention maps. Thus, attention maps from higher blocks can cover more extensive regions, and the lower blocks concentrate on smaller attribute regions of input images. However, methods based on attention mechanism are apt to be disturbed by complex surroundings and backgrounds. To alleviate the challenge, Yaghoubi et al.^[7] introduced a coarse attentive body segmentation module which multiplies features and ground truth masks to discriminate between the foreground and background. Whereas, attention masks fail to take the attribute-specific context into consideration, so the ablation studies^[7] find that coarse attention for the foreground regions is not helpful as their expectation. A popular solution is to embed inter-channel and spatial information of specific attribute feature maps. SE-Net^[9] squeezed each 2D feature map in simple manner to efficiently build inter-dependencies among channels. CBAM^[10] further advanced this idea by encoding spatial information and managing channel extraction and spatial encoding in two independent processes. The inevitable information loss has happened since both of them squeeze their channel dimension for inter-relationships. Taking inspiration from CBAM, two processes have been aggregated into one in our paper which captures channel dependencies and preserves spatial information with the help of global max pooling and global average pooling.

3 Proposed Method

The overall framework of VALA is illustrated in Fig. 3. VALA consists of a main network, a view prediction branch and a regional attention branch. The main network is built to obtain generic features first, and features from shallow layers of the main network are input into the view prediction branch to predict four view confidences. The architecture of view prediction branch is shown in Fig. 4. View confidences are then delivered back to shallow layers for composing view-attributes. To localize a specific view-attribute, the attentive structure named regional attention is introduced to capture attribute corresponding region. View confidences and the output of regional attention are aggregated together

3.1 Network Architecture

During pedestrian attribute recognition, some global attri-

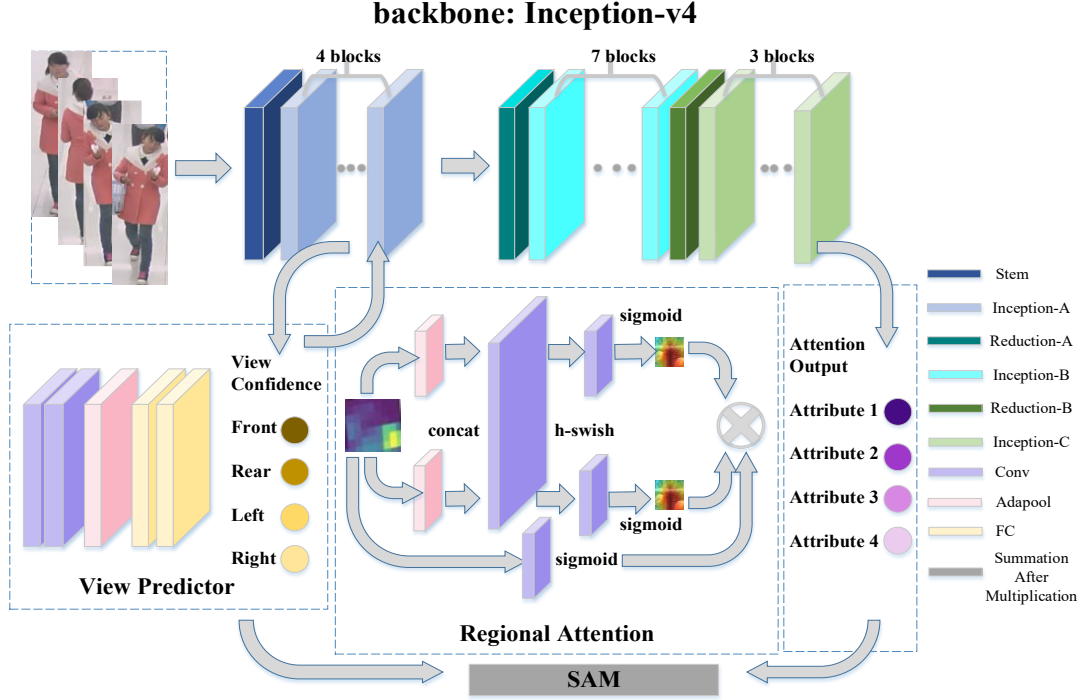


Fig. 3 Overall framework of VALA method. The primary network follows the structure of Inception-v4^[27], and Inception-ResNet-v2^[27] network is considered to replace Inception-v4 in training for rapid training speed. View prediction branch is constructed after Inception-A to gain four view confidences, while the regional attention is built after Inception-C to output attribute-corresponding regions as above. Eventually, the result is obtained by the above two branches via multiplication and summation. Different modules are annotated in different colors in the framework.

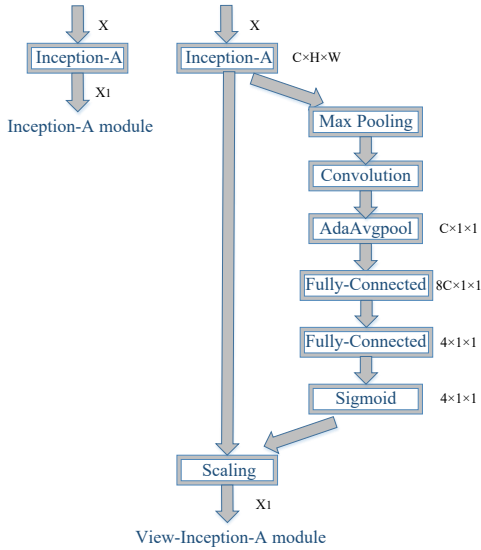


Fig. 4 Module architecture of Inception-A with embedding view prediction. Scaling contains upsampling operation.

butes rely on large convolutional kernels, while other local attributes are dependent on small convolutional kernels. Therefore, Inception-v4^[27] is adopted as the primary network which possesses different sizes of convolutional kernels for different scales of features in the same convolutional layer to obtain both global and local features simultaneously. Meanwhile, Inception-v4 is sufficiently deep for extracting semantically stronger features which has

a more uniform simplified architecture and more inception modules than Inception-v1-3^[28-30].

Inception-v4 mainly consists of Stem, Inception-A, Reduction-A, Inception-B, Reduction-B and Inception-C modules. Inspired by Google-Net (Inception-v1^[28]) which has two auxiliary classifiers, two auxiliary branches are transformed to view predictor and regional attention respectively in proposed method, but the position of our two branches are not corresponded to the original location in Google-Net. Furthermore, the average pooling layer, dropout layer and the final softmax in the original network are eliminated, and a BN layer is used directly to normalize final attribute recognition units instead.

Since Inception-v4 network tends to be very deep, it is natural to combine Inception architecture with residual connections which accelerate the training process of Inception network to explore deeper feature layers. Inception-ResNet-v2 is also trained as our main network to speed up the inference process of our model.

3.2 View Predictor

When monitoring cameras are manipulating, the positions of the same attribute from recorded images vary across different views. Furthermore, the relationship between views and attributes is explicit that unique visual clues can help the recognition of pedestrian attributes to some extent. Based on the shared feature maps output by Inception-A, VALA constructs a view prediction branch to forecast views confidences for attributes. For input feature maps F_1 ,

pooling and convolution layers are responsible for removing redundant information. Subsequently, the convolution layer is followed by an adaptive average pooling which downsamples the feature maps to intermediate variable F' , in order to deliver F' into fully-connected layer. To explore larger receptive field for feature maps, convolution and adaptive average pooling are applied in view predictor to reshape feature maps into 1×1 instead of allowing one convolution to resize directly. Then, F' is passed through two fully-connected layers. Let $Y_{vp1} = [f, b, l, r]$ denotes predicted view confidences, mathematically, Y_{vp1} can be represented by following equations:

$$Y_{vp1} = \sigma(W_{fc2} \cdot W_{fc1} \cdot F') \quad (1)$$

where \cdot means the dot product of two matrices, W_{fc1} and W_{fc2} are the weight matrices of the two fully-connected layers. Activated by sigmoid function, Y_{vp1} is a four-dimensional output which is then fed back to Inception-A blocks. As depicted in Fig. 4, the specific view-attribute is then composed by extracted feature in Inception-A and view confidences. The composed view-attribute participates in further deep feature extraction, which constructs the relevance of shallow and deep networks and supervises the network to focus on attribute-specific regions.

The predicted view confidences are also delivered to the final classification units as the view weights for attribute from different views to guide attribute recognition. Replacing the activation function by softmax function, let Y_{vp2} denote delivered view information, and it can be formulated as:

$$Y_{vp2} = \text{softmax}(W_{fc2} \cdot W_{fc1} \cdot F') \quad (2)$$

3.3 Regional Attention

Later studies^[9,10] have confirmed that inter-channel dependencies and spatial attribute information of input attribute-features have the influence on the accuracy of spatial channel integration and attribute related-areas localization. It shows concretely that attributes always correlate to different spatial locations of images^[3,5]. When the ratios of attributes are different, every channel inter-dependence of attribute-features should have an adjustment. However, most previous methods^[9,10] which use channel attention and spatial attention have problem in achieving greater performance. CBAM^[10] has difficulty in handling the relationship between channel attention and spatial attention since the two processes are computed independently. Motivated by the way to build spatial attention, our regional attention addresses this problem by utilizing global max pooling and global average pooling to preserve spatial attribute attention and channel interaction simultaneously. The structure of our regional attention is shown in Fig. 3. The outcome of Inception-C is taken as the input of regional attention, and regional attention is factorized into three small branches. Since the pedestrian is shown in a standing posture from the input image which is not flipped, the whole position of the pedestrian occupies in the largest pixels in the height orientation. Therefore, before localizing a specific view-

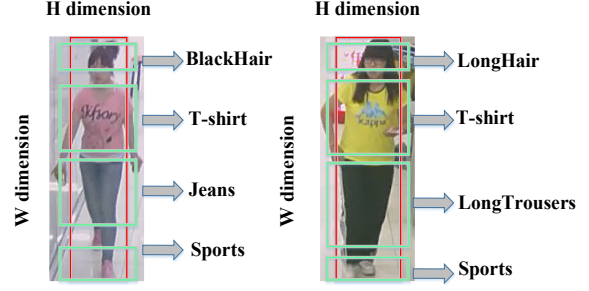


Fig. 5 Examples of localization operation by height and width branches. Images are from RAPv2 dataset^[11], and red regions are produced in height dimension, while green regions are generated in width dimension.

attribute, it needs to affirm the position of the pedestrian in the height orientation and to eliminate the interference of background firstly.

The global pooling is often used to encode spatial information, but it squeezes both space-related dimensions of height and width that causes positional information loss. To make regional attention attribute interactions spatially, we utilize the capability of global max pooling (GMP) in texture feature extraction to apply a spatial extent of adaptive kernels to embed local spatial attribute information along the height dimension and eliminate redundant data. Since corresponding regions of different attributes distribute in different positions of a pedestrian, the width branch is built to find the spatial information of related positions for the corresponding attribute in width dimension. For the width branch, adaptive global average pooling (GAP) is conducted to preserve global spatial attribute information along width dimension without any channel reduction for keeping as much spatial information as possible. Concrete localizing operation examples of height and width branches are displayed in Fig. 5. The output feature maps from the two small branches retain the channel dimension unchanged compared with the input, and they can be formulated as follows:

$$GMP(x) = \max_w(x(h, i)) \quad (3)$$

$$GAP(x) = \frac{1}{H} \sum_{j=1}^H(x(j, w)) \quad (4)$$

The above two pooling functions make up spatial attribute feature aggregation in our method, and the unchanged channel dimension, which is different from previous shrinking operation can make attribute information loss as few as possible. Subsequently, we permute the height and width dimension of the average pooled features and integrate the outputs of the two small branches along space-related dimension. To conduct spatial attribute information of the two small branches to complement each other, the integrated result is passed through a convolution to output the intermediate result F' , which is activated by h-swish function^[31]. Based on ReLU6 function, h-swish function eliminates latent precision loss and improves the efficiency in deep network particularly. The intermediate output can be represented by the following equation:

$$F' = h - \text{swish}(f(\text{concat}(GMP(x), GAP(x))) \quad (5)$$

where f stands for the convolutional operation, F' is defined as the intermediate vector. Then we remould the intermediate vector back to two attribute-feature vectors, which are the same size as original pooled features. To modulate the inter-channel dependencies for specific attributes, another two convolution transformations are utilized to augment channel dimension into C , which represents the class number in final attribute recognition units. Through a sigmoid activation layer, two attribute-feature maps gradually generate two attention maps of specific attributes in different spatial positions. Meanwhile, the third branch named *ratio-balance* branch is constructed to balance the ratio of the above two space-related branches by gaining the weights of two attention maps. All three branches are aggregated together via multiplication, and the output can be regarded as the whole attention weights of the view-attribute in the corresponding area. Set Y_a as the output of regional attention. The above operation can be written as:

$$Y_a = \sigma(f_3(F)) \times \sigma(f_1(F_1)) \times \sigma(f_2(F_2)) \quad (6)$$

where σ is the sigmoid function, F_1 and F_2 are the split feature vectors from intermediate vector F' in the height and width dimension respectively, while F is the initial input attribute features from Inception-C blocks. f_1, f_2 and f_3 represents the convolution operations to handle F_1, F_2 and F .

View confidences are taken as the contribution of view prediction branch, and Y_a is treated as the contribution of regional attention. By Combining view contribution with attention contribution to obtain the final attribute recognition, the attentive localization of a specific view-attribute can be realized.

4 Experiments

We assess our method on three public datasets, including RAP^[12], RAPv2^[11], and PA-100K^[13]. Specifically, our experiments are separated into four parts: (1) comparative experiment in RAP and RAPv2 datasets, (2) transfer learning of view predictor in PA-100K datasets, (3) ablation study in RAPv2 datasets, (4) pedestrian attribute recognition experiment in real surveillance scenarios.

4.1 Datasets

RAP dataset^[12] is collected from real indoor surveillance scenarios, and 26 cameras are selected to acquire all 41585 samples. Each image of this dataset is annotated with 72 fine-grained attributes and extra contextual factors including viewpoints, occlusion and body parts.

RAPv2 dataset^[11] comes from a realistic surveillance scenarios at a shopping mall, and all 84928 images which contain 2589 person identities are captured by 25 cameras. Viewpoint attribute is also contained in RAPv2.

PA-100K dataset^[13] is known to become the largest dataset in pedestrian attribute recognition domain for 100000 images in total captured from 598 real outdoor surveillance cameras. According to a ratio of 8:1:1, PA-100K dataset is randomly split into training, validation, and testing sets, and each image is labeled by 26 attributes.

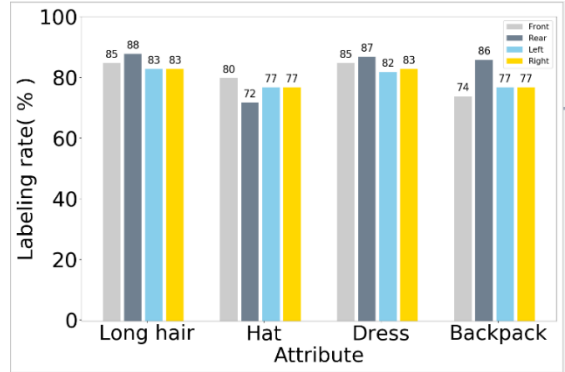


Fig. 6 Labeling rates of some typical attributes from different views in RAPv2 dataset^[11]. Typical attributes are long hair, hat, dress and backpack.

4.2 Evaluation Metrics

Two types of evaluation metrics are adopted in our experiment. (1) Label-based: the mA ^[32] criterion can be formulated as:

$$mA = \frac{1}{2N} \sum_{i=1}^M \left(\frac{TP_i}{P_i} + \frac{TN_i}{N_i} \right) \quad (7)$$

where N is the number of examples and M is the number of attributes. TP_i and TN_i are the number of correctly predicted positive and negative samples of the i -th attribute respectively. P_i and N_i are the number of positive and negative samples respectively. (2) Instance-based: the criteria of accuracy, precision, recall and F1 score^[12] are adopted, which are defined as follows:

$$Accuracy = \left(\frac{TP_i + TN_i}{P_i + N_i} \right) \quad (8)$$

$$Precision = \left(\frac{TP_i}{TP_i + FP_i} \right) \quad (9)$$

$$Recall = \left(\frac{TP_i}{TP_i + FN_i} \right) \quad (10)$$

$$F_1 = \left(\frac{2 \times Precision \times Recall}{Precision + Recall} \right) \quad (11)$$

where FP_i and FN_i are the number of incorrectly predicted positive and negative samples of the i -th attribute respectively.

4.3 Loss Function

Two types of cost functions are adopted in the training of the entire method. The first relates to the view prediction, and the second relates to attribute recognition. For the first cost function, the following negative log-likelihood is used.

$$Loss_{vp} = -\frac{1}{4L} \sum_{l=1}^L \sum_{k=1}^K \sum_{t=1}^{T=4} V_{k,l}^t \log \widehat{V}_{k,l}^t \quad (12)$$

where in Eq. 12, L and K denote the number of images and attributes respectively. T is the number of views, here is equal to 4. $V_{k,l}^t$ indicates the ground truth label of i -th view of k -th attribute in l -th image, and $\widehat{V}_{k,l}^t$ is the assumed prediction of view information.

Table 1 Comparative results of our proposed method and some state-of-the-art works on RAP dataset^[12]. Five categories of all methods are also listed in detail. The **best** results are highlighted in bold, and the second best results are underlined

Dataset		RAP					Category
Method	Metrics	mA	Accu	Prec	Recall	F1	
ACN ^[2]		69.66	62.61	80.12	72.26	75.98	Global-based: Multi-attribute joint prediction
DeepMAR ^[16]		73.79	62.02	74.92	76.21	75.56	
PGDM ^[3]		74.31	64.57	78.86	75.90	77.35	Part-based: Pose estimation as the auxiliary supervision
DTM+AWK ^[17]		<u>82.04</u>	67.42	75.87	<u>84.16</u>	79.80	
JRL ^[18]		74.74	-	75.08	74.96	74.62	Sequential prediction-based: Joint recurrent learning of attribute context and correlation by LSTM module
GRL ^[19]		81.20	-	77.70	80.90	79.29	
HP-Net ^[13]		76.12	65.39	77.33	78.79	78.05	Attention-based: Multi-scale attention mechanism Attention mask prediction
Da-HAR ^[8]		84.28	59.84	66.50	84.13	74.28	
VeSPA ^[33]		77.70	67.35	79.51	79.67	79.59	Attribute-based: Visual prediction
ALM ^[20]		81.87	68.17	74.71	86.48	<u>80.16</u>	Attribute related-region localization
Our VALA		78.33	<u>67.48</u>	<u>79.81</u>	80.84	80.32	View predictor + Attention mechanism + Attribute related-region

Table 2 Comparative results of our proposed method and some state-of-the-art works on RAP-2.0 dataset^[1]. Results* of DIAA^[6], VAC^[34], and ALM^[20] are reimplemented by Jia et al.^[35]. The **best** results are highlighted in bold, and the second best results are underlined

Dataset		RAPv2				
Method	Metrics	mA	Accu	Prec	Recall	F1
DIAA ^[6] *		<u>77.87</u>	<u>67.19</u>	79.03	79.79	79.04
VAC ^[34] *		76.74	67.52	<u>80.42</u>	78.78	<u>79.24</u>
ALM ^[20] *		78.21	66.98	78.25	80.43	78.93
Strong Baseline ^[35]		77.34	66.12	81.99	75.62	78.21
Our VALA		77.38	66.23	78.80	<u>79.80</u>	79.30

The following weighted cross-entropy loss^[16] is utilized as the loss for attribute recognition.

$$Loss_a = -\frac{1}{N} \sum_{i=1}^N \sum_{j=1}^M w_j (y_{i,j} \log(\sigma(\widehat{y}_{i,j})) + (1 - y_{i,j}) \log(1 - \sigma(\widehat{y}_{i,j}))) \quad (13)$$

$$w_j = \begin{cases} e^{1-r_j} & y_{i,j} = 1 \\ e^{r_j} & y_{i,j} = 0 \end{cases} \quad (14)$$

where N and M denote the number of images and attributes respectively, $y_{i,j}$ indicates the ground truth of j -th attribute in i -th image, and $\widehat{y}_{i,j} \in \{0,1\}$ is the predicted result. w_j in Eq. 14 denotes the weight for j -th attribute to alleviate the imbalanced distribution of positive and negative samples^[3], and r_j is the proportion of positive samples of j -th attribute.

The final loss function is calculated as follow:

$$Loss = \alpha Loss_{vp} + \beta Loss_a \quad (15)$$

α and β are hyper-parameters to balance the two different loss.

4.4 Implementation Details

In our experiments, the average pooling layer, dropout layer and the final softmax from original Inception-v4^[27] structure are eliminated, and a BN layer is added in final attribute recognition units to balance the change. Without other tricks, only the random crop strategy is employed to

augment data for avoiding data unbalanced and over-fitting. During training process, the images are resized and normalized into 256×192 , and SGD optimizer is utilized with a batch size of 64, a momentum of 0.9, and a weight decay of 5×10^{-5} . When handling shallow view features, the learning rate is set to 0.1, while the learning rate equals 0.01 in deeper training. Our model is trained on four NVIDIA 2080Ti GPUs based on Pytorch environment.

4.5 Comparative Experiment

We compare our VALA approach on RAP dataset^[12] with a great number of state-of-the-art pedestrian attribute recognition methods, e.g. ACN^[2], DeepMAR^[16], VeSPA^[33], HP-Net^[13], JRL^[18], GRL^[19], PGDM^[3], ALM^[20], Da-HAR^[8] and DTM+AWK^[17]. These PAR algorithms place emphasis on different aspects: global-based, part-based, attention-based, sequential-based, and attribute-based. The comparative results of our VALA and other methods on RAP dataset is displayed in Tab. 1.

The results shows that our proposed method achieves competitive performances under both label-based and instance-based metrics on RAP dataset. As for F1score, VALA surpasses all state-of-the-art methods with 80.32%. Though, in term of accuracy and precision, the proposed method wins the second best results, its scores lag only 0.69% and 0.31% behind the best methods ALM^[20] and ACN^[2] respectively. Compared with the previous methods relying on multi-attribute joint prediction, our proposed method can reach significant improvement. A higher mA score about 4.02% is performed than the part-based method PGDM^[3], which demonstrates the effectiveness of taking view features as prior knowledge. We find that our VALA does achieve better gains than VeSPA^[33] which belongs to view prediction and classifies the dataset by different views for training. The main reason is that the capability of our regional attention is utilized to localize the representative related areas of specific attributes from different views rather than to distinguish different view images manually. Better performances of our VALA are seen from comparison between these two methods on PA-100K dataset. Since more recent methods begin to focus on attention mechanism or

Table 3 The transferable capability of our view predictor and attribute classification model on PA-100K dataset^[13] with bold best result and underline second best result. The results are obtained by fixing the parameters of view predictor trained on RAP dataset and retraining our attribute inference model.

Dataset		PA-100K				
Method	Metrics	mA	Accu	Prec	Recall	F1
DeepMAR ^[16]		72.70	70.39	82.24	80.42	81.32
HP-Net ^[13]		74.21	72.19	82.97	82.09	82.53
VeSPA ^[33]		76.32	73.00	84.99	81.49	83.20
PGDM ^[3]		74.95	73.08	84.36	82.24	83.29
LG-Net ^[5]		76.96	75.55	<u>86.99</u>	83.17	85.04
ALM ^[20]		<u>80.68</u>	77.08	84.21	<u>88.84</u>	86.46
DTM+AWK ^[17]		81.63	77.57	84.27	89.02	86.58
MT-CAS ^[36]		77.20	<u>78.09</u>	88.46	84.86	<u>86.62</u>
Our VALA		80.08	78.14	<u>87.60</u>	86.73	87.16

attribute-related localization, our proposed method still get comparable results, and our attention branch has the potential to trace attribute-corresponding regions.

Comparative experiment is also brought about on RAPv2 dataset^[1]. Since RAPv2 dataset is not as universal as RAP dataset, we only compare our method with some recent works including DIAA^[6], VAC^[34], ALM^[20] and Strong Baseline^[35]. As shown in Tab. 2, our VALA obtain the best result in F1score and the second best result in recall matrix, which illustrates the comparable and potential capability of our method in pedestrian attribute recognition.

4.6 Transfer Learning Analysis

Owing to the peculiar viewpoint labels of RAP and RAPv2 datasets, our view predictor has been well trained. To verify the applicability of view prediction and view feature supervision and reflect the benefit of view-attribute, we fix the parameters of all view prediction trained on RAP dataset^[12], and retrain attribute recognition model to conduct transfer learning on PA-100K dataset^[13]. LG-Net^[5] and MT-CAS^[36] are appended to complement the comparative methods.

As shown in Tab. 3, the proposed method achieve better performance on PA-100K dataset compared with existing state-of-the-art methods. Our proposed method outperforms all previous methods in term of accuracy and F1 scores, improving 0.05% and 0.54% upon the second best method MT-CAS^[36] respectively. Meanwhile, our VALA also win the second best result with 87.60% in precision. Moreover, VALA has a comparable mA matrix, which is not much worse than the method^[17,20] put forward recently. Notably, VALA manifests a competitive performance with a significant margin, especially compared with the single visual model. These consequence attributes to the benefit of our regional attention which embeds inter-channel dependencies and preserves spatial attribute information to localize attrib-

Table 4 Further complexity comparisons among a sequence of different backbone networks in RAP dataset^[12]. The parameters are the whole parameters of their models, while the F1 scores are produced by their single backbones.

Method	Backbone	Params	F1
Strong Baseline ^[35]	ResNet50	23.6M	78.94
VeSPA ^[33]	Google-Net	17.0M	74.58
ALM ^[20]	BN-Inception	17.1M	78.20
GRL ^[19]	Inception-v3	>50M	78.30
Our VALA	ResNet50	32.8M	76.19
	Inception-v4	59.3M	77.72
	Inception-ResNet-v2	59.3M	77.90

ute-corresponding regions from different views. The improvement of transfer learning results on PA-100K dataset illustrates the strong transferable capability of view prediction branch and the stable ability of composed view features to contact shallow with deep feature and to guide the process of deep feature extraction.

4.7 Complexity Analysis

The design of Inception-v4 as our baseline can extract deeper attribute features, but enormous parameters is inevitably produced by the Inception-v4 structure and other branches. When sophisticated parameters are deployed on devices, the speed of training process may drop and the time of inference may increase. Complexity Analysis of the Inception-v4 baseline is depicted in Tab. 4, the rest of approaches which use Inception series networks as their backbone are VeSPA^[33], ALM^[20] and GRL^[19], while ResNet50^[11] is utilized in Strong Baseline^[35]. The parameters in Tab. 4 are the whole parameters in their models, but the F1 scores are produced by their single baselines.

We find that the proposed VALA module increases the number of parameters significantly which are mainly caused by the baseline, namely Inception-v4. The intention to only apply Inception-v4 for deeper specific attribute-feature extraction has not achieved the desired result with only 77.72% in F1 metric, which lags behind most of mentioned method, even Strong Baseline^[35] method with a more simple backbone ResNet50. The main reason may be the depth and complexity of the network that prevent us from optimizing the parameters for the optimal effect. However, when the backbone of our VALA is replaced with ResNet50, the performance has a serious drop to 76.19% in F1 metric, which is 1.53% lower than the F1 score that Inception-v4 produces. Because ResNet50 is not deep sufficiently for view features to contact deep feature information and for regional attention to conduct deep localization. Since Inception-v4 tends to be very deep, it is natural to replace it with Inception-ResNet-v2^[27] to reap the benefit of the residual approach and to retain its computational efficiency concurrently. We retrain our model on Inception-ResNet-v2

Table 5 Ablation study on RAPv2 dataset^[1]. All components is added gradually. Here, VF refers the embedded view-feature, VP refers the operation that add view prediction to final attribute recognition units, while VFB+VPB refers the operation that place view-feature and view prediction at the end of Inception-B module. RA is our regional attention, RAB is the operation that put regional attention at the end of Inception-B module, RAH is the regional attention without width branch, similarly, RAW is the regional attention without height branch.

Model \ Metric	mA	Accu	Prec	Recall	F1
Baseline	74.32	62.97	77.02	76.58	76.80
Baseline+VF	75.92	64.33	77.10	77.92	77.51
Baseline+VF+3VP	75.98	64.52	77.21	78.03	77.62
Baseline+VF+4VP	76.20	64.74	77.21	78.34	77.77
Baseline+RA	76.32	65.30	77.93	78.50	78.21
Baseline+VF+4VP+SE	76.31	65.34	78.01	78.51	78.26
Baseline+VF+4VP+CBAM	76.39	65.38	78.12	78.52	78.32
Baseline+VF+4VP+RAH	75.90	64.79	77.72	78.40	78.06
Baseline+VF+4VP+RAW	76.88	65.83	78.19	79.34	78.76
Baseline+VFB+4VPB+RA	76.98	65.90	78.22	78.91	78.56
Baseline+VF+4VP+RAB	76.51	65.67	77.83	78.80	78.31
VALA(Ours)	77.38	66.23	78.80	79.80	79.30

baseline to get slightly higher F1 score and obviously quicker training speed.

4.8 Ablation Study

Ablative experiment is set to justify the contribution per block and each component is appended gradually. As shown in Tab. 5, starting with the Inception-v4 baseline, we compare our method with several variants.

The capability of prior view information: Based on the baseline, view feature supervision is added first, and an impressive promotion has been found which demonstrates the capability of view feature to have a connection between shallow feature and deep feature. Then, three view confidences (namely abandon the right view) are added to attribute recognition units as the view weights, and a slightly improvement is gained which illustrates the feasibility of considering view information as prior knowledge to guide final attribute recognition. Then the abandoned right view is set back for the purpose of supplying full views (namely the same view setting as our VALA). Since an input image are

not flipped, attribute from right view can be regarded as the mirror flipping for attribute from left view to augment data. Considering the view completeness, four views module still has a comparable capability, though relatively few improvement is yielded by an additional right view.

The capability of regional attention: On the basis of acquiring visual clues as the auxiliary supervision, we replace the attention module in proposed method with SE-Net and CBAM to evaluate the capability of our regional attention to obtain attribute-related areas for different view features. When SE-Net^[9] and CBAM^[10] capture view feature maps from the stacking Inception-C blocks, their effects of localizing view-attribute related regions are quite equivalent, but far from the effect performed by our regional attention. This fact verifies that embedding inter-channel dependencies and preserving spatial attribute information in one process truly have an important impact on the aspect of attribute-corresponding region localization, which is crucial for more precise attribute recognition. Furthermore, the contribution of internal branches of regional attention is also explored, and two variants are constructed. Compared with our VALA, the F1 score fall to 78.06% with 1.24% margin when the width branch is removed, while the F1 score of regional attention without height branch is lower than our method with 0.54% margin. The reason of this phenomenon is that the spatial information capturing of a specific view attribute plays a more important role in attribute-related region localization.

The contribution of two branches in the whole method:

In this category, we evaluate the contribution of two branches, and each branch is appended gradually. Comparing with the model without viewpoint component (Baseline+RA), the result of our VALA is explicitly improved in all evaluation criteria with 1.06% in mA, 0.93% in accuracy, 0.87% in precision, 1.30% in recall and 1.09% in F1 score. The greater result demonstrates the feasibility of considering viewpoint information to assist the attribute recognition performance. When regional attention is removed (Baseline+VF+4VP), a more severe drop has happened even though other setting is kept unchanged, which further explains that visual attribute localization is more significant for attribute recognition. In regard to the above two models with either of them, we find that the improvement of performance produced by attention mechanism is higher than that generated by view prediction. The remarkable evaluation indicates that it is important to accurately localize view-attribute after capture it for better attribute recognition effect. Visualization of some attribute attentive areas in Fig. 7 shows the contribution of two modules specifically.

The layers to export features for two branches: In our original implementation, we get shallow feature maps for view prediction from the output of stacking Inception-A blocks, while deep feature maps are exported from stacking Inception-C blocks. According to the empirical thought, the Inception-A and Inception-C layers in the entire Inception network is thought to be either shallow or deep sufficiently for view extraction and attention localization. However, it is

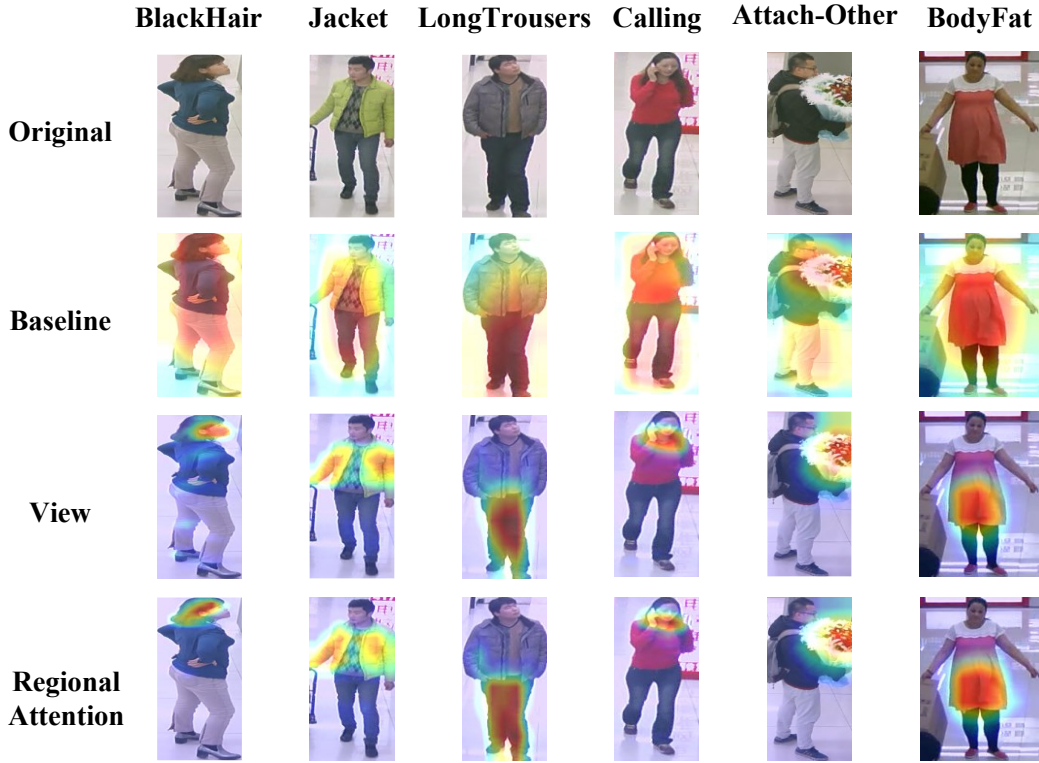


Fig. 7 Attention heatmaps generated by single baseline, view supervision and regional attention. The example images are from RAPv2 dataset^[1], and attributes to be located are *BlackHair*, *Jacket*, *LongTrousers*, action-*Calling*, attachment-*Other*, *BodyFat* in each column.

still necessary to explore which layer can meet more satisfied demand. We rearrange the position of view prediction branch to the end of Inception-B blocks and keep the attention branch position unchanged. Comparing with our original setting, a drop result indicates that feature maps in Inception-A are more holistic and more appropriate for extracting global view information. Referring to the first experimental result, the position of view prediction is retained, but regional attention is assigned to the end of Inception-B blocks. The performance of our VALA still surpasses that of the variant, which confirms that encoding channel and spatial attribute information in relatively deeper layers can reach better achievement of the localization for local attribute-corresponding regions.

To sum up, ablation studies show that it is important to take the view information into consideration as a effective prior knowledge, which is conducive to the improvement of the pedestrian attribute recognition model performance. The introduction of the attention mechanism increases the fine-grained and overall performance of attribute recognition.

4.9 Pedestrian attribute recognition in Surveillance

In order to verify the actual recognition effect of our VALA model, we select pedestrian images from real video surveillance scenarios. Our model is pre-trained on RAP^[12] dataset, and some of the representative results are shown in Fig. 8. The results illustrate that even though no positioning information is included in the pedestrian images, the VALA model is also able to accomplish the identification of the sa-

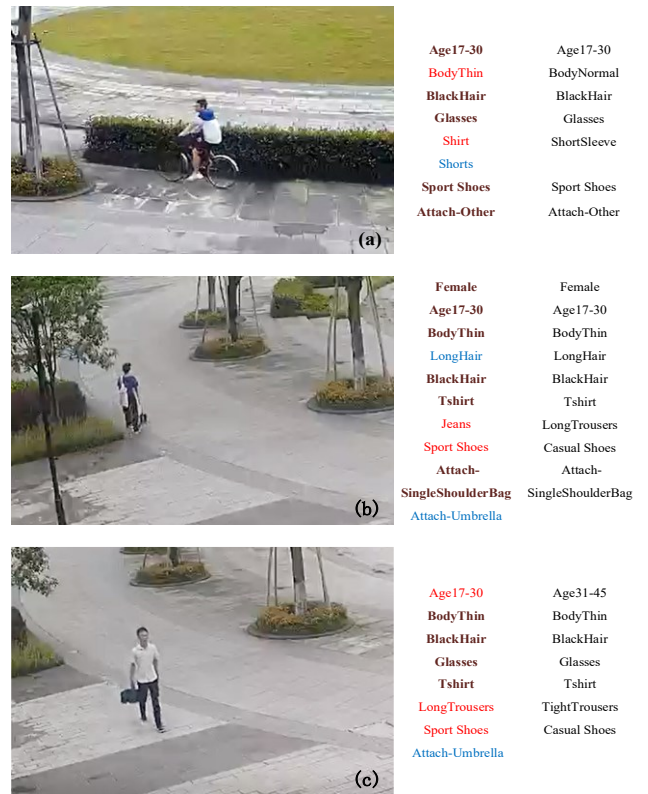


Fig. 8 Attribute recognition results of real pedestrian images in video surveillance scenarios. **Correct** attribute predictions are marked in bold font and brown, **missed** attributes in blue, **incorrect** predictions in red and ground truths in black.

me attribute from different views. For example, the view of the glasses attribute is side-view in Picture (a) and is front-view in (c), but both of them are successfully identified. Moreover, some local attributes like *BlackHair* have also been recognized, which demonstrates the accuracy for fine-grained classification in our model.

The VALA model adopts a multi-task learning framework as a whole, improving the identification performance of all attributes. It forecasts the pedestrian perspective through the view prediction, and then practices specific view-attribute recognition units. Compared with the localization of body parts, the view prediction based on global features is easier to train and the calculation cost is lower. The attribute classification units leverage the channel and spatial attention mechanism to guide the network to focus on the most representative view feature position, so that the attribute recognition performance is effectively improved.

5 Conclusion

We propose an attention-based pedestrian attribute recognition model, which can predict view information to compose view-attribute by view predictor and localize specific regions of view-attribute by attention mechanism. Utilizing the unique view tags of the RAP and RAPv2 datasets and the shallow convolution features of the Inception network, the view prediction is trained. To construct a view-specific attribute recognition unit, we introduce a channel and spatial attention mechanism to enhance feature discrimination and localize view-attribute for ameliorating recognition performance. In the comparative experiment on RAP and RAPv2 datasets, multiple indicators of the VALA model have reached the comparable results, which have confirmed the overall performance of the model. On PA-100K dataset, the applicability and stability of view-feature and view prediction are verified by the evaluation of transfer learning. In future research, we will pay more attention on the deployment possibilities of the pedestrian attribute recognition network model based on the framework of this article on mobile devices to achieve greater practical application value.

Acknowledgements

This work was supported by the National Key Research and Development Program of China (No. 2018YFB1308000)

References

[1] Li D, Zhang Z, Chen X, et al. A richly annotated pedestrian dataset for person retrieval in real surveillance scenarios[J]. *IEEE transactions on image processing*, 2018, 28(4): 1575-1590.

[2] Sudowe P, Spitzer H, Leibe B. Person attribute recognition with a jointly-trained holistic cnn Model[C]. *Proceedings of the IEEE International Conference on Computer Vision Workshop*, 2015: 87-95.

[3] Li D, Chen X, Zhang Z, et al. Pose guided deep model for pedestrian attribute recognition in surveillance scenarios[C]. *IEEE International Conference on Multimedia and Expo*, 2018: 1-6.

[4] Bourdev L, Maji S, Malik J. Describing People: A poselet-based

approach to attribute classification[C]. *International Conference on Computer Vision*, 2011: 1543-1550.

[5] Liu P, Liu X, Yan J, et al. Localization guided learning for pedestrian attribute recognition[J]. *arXiv preprint arXiv:1808.09102*, 2018.

[6] Sarafianos N, Xu X, Kakadiaris I A. Deep imbalanced attribute classification using visual attention aggregation[C]. *Proceedings of the European Conference on Computer Vision*, 2018: 680-697.

[7] Yaghoubi E, Borza D, Neves J, et al. An attention-based deep learning model for multiple pedestrian attributes recognition[J]. *Image and Vision Computing*, 2020, 102: 103981.

[8] Wu M, Huang D, Guo Y, et al. Distraction-aware feature learning for human attribute recognition via coarse-to-fine Attention Mechanism[C]. *Proceedings of the AAAI Conference on Artificial Intelligence*, 2020, 34(07): 12394-12401.

[9] Hu J, Shen L, Sun G. Squeeze-and-excitation networks[C]. *Proceedings of the IEEE Conference on Computer Vision and Pattern Recognition*, 2018: 7132-7141.

[10] Woo S, Park J, Lee J Y, et al. Cbam: Convolutional block attention module[C]. *Proceedings of the European conference on computer vision*, 2018: 3-19.

[11] He K, Zhang X, Ren S, et al. Deep residual learning for image recognition[C]. *Proceedings of the IEEE Conference on Computer Vision and Pattern Recognition*, 2016: 770-778.

[12] Li D, Zhang Z, Chen X, et al. A richly annotated dataset for pedestrian attribute recognition[J]. *arXiv preprint arXiv:1603.07054*, 2016.

[13] Liu X, Zhao H, Tian M, et al. HydraPlus-Net: Attentive deep features for pedestrian analysis[C]. *Proceedings of the IEEE International Conference on Computer Vision*, 2017: 350-359.

[14] Dalal N, Triggs B. Histograms of oriented gradients for human detection[C]. *IEEE computer society Conference on Computer Vision and Pattern Recognition*, IEEE, 2005, 1: 886-893.

[15] Layne R, Hospedales T M, Gong S, et al. Person re-identification by attributes[C]. In *Proceedings of the British Machine Vision Conference*, 2012, 2(3): 8.

[16] Li D, Chen X, Huang K. Multi-attribute learning for pedestrian attribute recognition in surveillance scenarios[C]. *IAPR Asian Conference on Pattern Recognition*, 2015: 111-115.

[17] Zhang J, Ren P, Li J. Deep Template Matching for Pedestrian Attribute Recognition with the Auxiliary Supervision of Attribute-wise Keypoints[J]. *arXiv preprint arXiv:2011.06798*, 2020.

[18] Wang J, Zhu X, Gong S, et al. Attribute recognition by joint recurrent learning of context and correlation[C]. *Proceedings of the IEEE International Conference on Computer Vision*, 2017: 531-540.

[19] Zhao X, Sang L, Ding G, et al. Grouping Attribute Recognition for Pedestrian with Joint Recurrent Learning[C]. *Proceedings of the Twenty-Eighth International Joint Conference on Artificial Intelligence*, 2018: 3177-3183.

[20] Tang C, Sheng L, Zhang Z, et al. Improving pedestrian attribute recognition with weakly-supervised multi-scale attribute-specific localization[C]. *Proceedings of the IEEE International Conference on Computer Vision*, 2019: 4997-5006.

[21] Zitnick C L, Dollár P. Edge boxes: Locating object proposals from edges[C]. *European conference on computer vision*, Springer, Cham, 2014: 391-405.

[22] Feng Z, Lai J, Xie X. Learning view-specific deep networks for person re-identification[J]. *IEEE Transactions on Image Processing*,

2018, 27(7): 3472-3483.

[23] Farfadi S S, Saberian M J, Li L J. Multi-view face detection using deep convolutional neural networks[C]. Proceedings of the 5th ACM on International Conference on Multimedia Retrieval, 2015: 643-650.

[24] Sadr H, Pedram M M, Teshnehlab M. Multi-view deep network: A deep model based on learning features from heterogeneous neural networks for sentiment analysis[J]. IEEE Access, 2020, 8: 86984-86997.

[25] Zhu F, Li H, Ouyang W, et al. Learning spatial regularization with image-level supervisions for multi-label image classification [C]. Proceedings of the IEEE Conference on Computer Vision and Pattern Recognition, 2017: 5513-5522.

[26] Tan Z, Yang Y, Wan J, et al. Attention-based pedestrian attribute analysis[J]. IEEE transactions on image processing, 2019, 28(12): 6126-6140.

[27] Szegedy C, Ioffe S, Vanhoucke V, et al. Inception-v4, inception-resnet and the impact of residual connections on learning[C]. Proceedings of the AAAI Conference on Artificial Intelligence, 2017, 31(1).

[28] Szegedy C, Liu W, Jia Y, et al. Going deeper with convolutions[C]. Proceedings of the IEEE Conference on Computer Vision and Pattern Recognition, 2015: 1-9.

[29] Ioffe S, Szegedy C. Batch normalization: Accelerating deep network training by reducing internal covariate shift[C].

International Conference on Machine Learning. PMLR, 2015: 448-456.

[30] Szegedy C, Vanhoucke V, Ioffe S, et al. Rethinking the inception architecture for computer vision[C]. Proceedings of the IEEE Conference on Computer Vision and Pattern Recognition, 2016: 2818-2826.

[31] Howard A, Sandler M, Chu G, et al. Searching for mobilenetv3[C]. Proceedings of the IEEE International Conference on Computer Vision, 2019: 1314-1324.

[32] Deng Y, Luo P, Loy C C, et al. Pedestrian attribute recognition at far distance[C]. Proceedings of the 22nd ACM international conference on Multimedia, 2014: 789-792.

[33] Sarfraz M S; Schumann A; Wang, Y, et al. Deep view-Sensitive pedestrian attribute inference in an end-to-end model[J]. arXiv preprint arXiv:1707.06089, 2017.

[34] Guo H, Zheng K, Fan X, et al. Visual attention consistency under image transforms for multi-label image classification[C]. Proceedings of the IEEE Conference on Computer Vision and Pattern Recognition, 2019: 729-739.

[35] Jia J, Huang H, Yang W, et al. Rethinking of pedestrian attribute recognition: realistic datasets with efficient method[J]. arXiv preprint arXiv:2005.11909, 2020.

[36] Zeng H, Ai H, Zhuang Z, et al. Multi-Task Learning via Co-Attentive Sharing for Pedestrian Attribute Recognition[C]. IEEE International Conference on Multimedia and Expo, 2020: 1-6.